MISR: A Multiangle Imaging SpectroRadiometer for Geophysical and Climatological Research from Eos

DAVID J. DINER, CAROL J. BRUEGGE, JOHN V. MARTONCHIK, THOMAS P. ACKERMAN, ROGER DAVIES, SIEGFRIED A. W. GERSTL, MEMBER, IEEE, HOWARD R. GORDON, PIERS J. SELLERS, JERRY CLARK, JAMES A. DANIELS, ERIC D. DANIELSON, VALERIE G. DUVAL, KENNETH P. KLAASEN, GERALD W. LILIENTHAL, DAVID I. NAKAMOTO, ROBERT J. PAGANO, AND TERRENCE H. REILLY

Abstract—**The scientific objectives, instrument concept, and data plan for the Multiangle Imaging SpectroRadiometer (MISR), an experiment proposed for the Eos Mission, are described. MISR is a pushbroom imaging system designed to obtain continuous imagery of the sunlit Earth at four different view angles (25.8°, 45.6°, 60.0°, and 72.5° relative to the vertical at the Earth's surface), in both the forward and aftward directions relative to nadir, using eight separate cameras. This strategy permits acquisition of multiangle imagery with uniform resolution (216 m for selected scenes; 1.73 km for global coverage) at the different angles, without gaps in spatial coverage. Observations will be acquired in four spectral bands, centered at 440, 550, 670, and 860 nm. Data analysis algorithms will be applied to MISR imagery to retrieve the optical, geometric, and radiative properties of complex, three-dimensional scenes, such as aerosol-laden atmospheres above a heterogeneously reflecting surface, nonstratified cloud systems, and vegetation canopies. The MISR investigation will address a number of scientific questions concerning the climatic and ecological consequences of many natural and anthropogenic processes, and will furnish aerosol information necessary for atmospheric corrections of surface images.**

I. Introduction

AMONG THE scientific issues to be addressed by the Earth Observing System (Eos) are the effects of geophysical processes and human activities on the Earth's ecology and climate. Through alteration of surface albedos, changes in surface and atmospheric chemistry, and modification of atmospheric aerosol content and cloudiness, such processes as desertification, deforestation, soil erosion, pollution, and volcanism can significantly, perhaps adversely, impact the Earth's energy budget and our environment. A detailed understanding of the causes and effects of regional and global change requires long-term monitoring of the atmosphere-land-ocean system coupled with development of realistic models. To carry out research in these areas, we have proposed the Multiangle Imaging SpectroRadiometer (MISR) as a nonfacility instrument investigation in response to the Eos Announcement of Opportunity. MISR has been specifically designed to acquire multispectral images of the *angular* reflectance signatures of terrestrial scenes. By combining ground processing software with a novel instrument design, MISR will obtain geometrically registered reflectance images having identical resolution at several view angles for the entire planet, without gaps in coverage. To our knowledge, this methodical approach is not feasible with any other instrument in the Eos mission configuration.

Specific instrument parameters are as follows:

View angles at Earth surface:	25.8°, 45.6°, 60.0°, 72.5°
Spatial resolution:	216 m for selected scenes (Local Mode) 1.73 km for global coverage (Global Mode)
Spectral bands:	440, 550, 670, 860 nm
Spectral bandwidths:	20–60 nm
Swath width:	210 km (443 km at equator for selected cameras)
Global repeat time:	16 days
Signal/noise ratio (10 percent albedo):	260 (Local Mode) 1880 (Global Mode)
In-flight radiometric accuracy:	3 percent using source- and detector-based calibration
Data rate:	222 kbps (Global Mode) 2 Mbps (Local Mode)
Power:	77 W
Mass:	75 kg.

Manuscript received June 2, 1988; revised August 29, 1988. This work was supported in part by the Jet Propulsion Laboratory, California Institute of Technology, under contract with the National Aeronautics and Space Administration.

D. J. Diner, C. J. Bruegge, and J. V. Martonchik are with the Jet Propulsion Laboratory, California Institute of Technology, Pasadena, CA 91109.

T. P. Ackerman is with Pennsylvania State University, University Park, PA 16802.

R. Davies is with McGill University, Montreal, Province of Quebec, H3A 2K6, Canada.

S. A. W. Gerstl is with Los Alamos National Laboratory, Los Alamos, NM 87545.

H. R. Gordon is with the University of Miami, Coral Gables, FL 33124.

P. J. Sellers is with the University of Maryland and Goddard Space Flight Center, Greenbelt, MD 20771.

J. Clark, J. A. Daniels, E. D. Danielson, V. G. Duval, K. P. Klaasen, G. W. Lilienthal, D. I. Nakamoto, R. J. Pagano, and T. H. Reilly are with the Jet Propulsion Laboratory, California Institute of Technology, Pasadena, CA 91109.

IEEE Log Number 8825536.

0196-2892/89/0300-0200$01.00

II. Science Objectives

A. Aerosols

Under normal background conditions, most of the atmospheric aerosol resides in the troposphere. Natural sources (e.g., dust storms, biogenic emissions, forest and grassland fires, and sea spray) account for about 90 percent of this aerosol, with the rest resulting from anthropogenic activity [1]. The opacity of the background tropospheric aerosol is typically 0.1 at visible wavelengths [2]. The amount of stratospheric aerosol is controlled by the size and frequency volcanic eruptions. In quiescent periods, the stratospheric opacity may be as low as a few hundredths. However, after even moderate eruptions such as that of El Chichon, opacities may reach a few tenths on a global basis and substantially higher values regionally [3]. Typically timescales for volcanic aerosol clouds are a few years.

The climatic impact of aerosols remains a matter of some debate. Model simulations of the effects of global aerosols typically predict surface temperature coolings on the order of a few °C [4], [5]. For comparison, the "Little Ice Age" of the 15th–19th centuries was characterized by average temperatures in Western Europe roughly 1°C cooler than present [6]. Observational evidence [7], [8] suggests an increase in the tropospheric aerosol burden at midlatitudes and in the Arctic, probably as the result of anthropogenic activities. Because anthropogenic aerosols usually contain carbonaceous material, they tend to have lower values of single-scattering albedo, $\bar{\omega}_0$, than natural aerosols. Waggoner *et al.* [9] report values of $0.54 < \bar{\omega}_0 < 0.61$ for urban industrial regions, $0.73 < \bar{\omega}_0 < 0.87$ for urban residential regions, and $0.89 < \bar{\omega}_0 < 1$ for rural areas. Along with the aerosol opacity, size distribution, and surface albedo, $\bar{\omega}_0$ determines the relative importance of backscatter and absorption, with regionally variable consequences for the surface radiation budget [10]. For example, surface radiation measurements show that haze aerosols over the Eastern U.S. cause an average 7-percent *reduction* in insolation [11], while measurements of the absorption of solar radiation by pollutant haze in the Arctic atmosphere [12] show a clear *increase* in the amount of solar energy deposition. Thus, at our present level of understanding the global climatic significance of particulate pollution is indeterminate [13] and a systematic, global monitoring program is needed. An increase in the amount of anthropogenic aerosols also poses a direct threat to the biologic and economic health of our environment. Industrial pollution is not the only source of concern. For example, slash-and-burn agriculture causes the loss of nearly 2×10^5 km^2 of natural forest each year, increases the CO_2 content of the atmosphere, and produces large-scale hazes over areas of Brazil, Africa, and Asia [6]. Desertification of the Earth's continents increases the mean surface albedo and potentially furnishes a fresh source of tropospheric aerosol. For example, windblown dust from the African Sahara has been observed over the Atlantic Ocean [14].

MISR will provide globally distributed estimates of aerosol amounts and optical characteristics that are necessary to investigate the effects of hazes, dust layers, and particulate plumes on the solar radiation budget and to monitor long-term trends in regional and global aerosol loadings.

B. Atmospheric Corrections of Land Surface Imagery

It is well established that scattering and absorption by aerosols are responsible for dramatic modifications of the spectral content of remotely sensed images of the Earth's surface, leading to classification errors [15] and reduced accuracy of image products such as vegetation maps [16]. Attenuation of the incident and reflected beams is offset by diffuse radiation that has been 1) reflected by the atmosphere without reaching the surface, 2) subjected to multiple reflections between the atmosphere and surface, and 3) scattered into the line-of-sight from neighboring terrain. The latter phenomenon, known as the "adjacency effect" [17]–[19], is of particular concern for biological productivity and water quality assessments of inland aquatic resources. Because of their low reflectance, the top-of-atmosphere (TOA) spectra of these targets are susceptible to contamination by radiation scattered from the surrounding brighter terrain. The heterogeneity of the surface reflectance and turbidity of inland waters preclude the use of marine atmospheric correction algorithms [20]. Other techniques that have been proposed required some *a priori* knowledge of the optical properties of the atmosphere or surface, but do not address how this information is to be acquired [14], [21]–[23]. Moreover, if the ground is (incorrectly) assumed to be lambertian, absolute surface reflectances derived from TOA radiances in certain view directions will contain potentially significant errors, even if the atmospheric state is known exactly [24].

Determination of aerosol scattering properties and multiangle measurements of nonlambertian scene reflectances with MISR will provide the information needed to implement accurate atmospheric corrections over land surface scenes.

C. Clouds

As a result of their large areal extent, high albedo, and variability on many timescales, clouds play a major role in governing the Earth's energy balance. Current theories and models of the response of the Earth's climate system to, for example, the increase in trace gases, are severely limited by our present ignorance of the feedback processes associated with changes in cloud amount and cloud properties. In this respect, two issues are paramount. One is the realistic modeling of cloud-radiation interaction taking into account the variable structure of broken cloud fields and processes that occur at the sub-grid scale level of present general circulation models. The other is the ability to invert satellite measured radiances to obtain hemispherical fluxes with sufficient resolution to discriminate between cloud-filled and cloud-free scenes.

Many theoretical studies have established that plane

parallel representations of cloud fields introduce large errors in the parameterization of radiation for climate models [25], [26]. It is currently recognized that cloud modeling must consider not only the effects of individual cloud shape but interactions such as shadowing and multiple scattering between clouds. Diffusion of radiation through the cloud sides and side illumination causes the bidirectional reflectance distribution functions (BRDF's) of cumuliform cloud fields to differ markedly from those of stratiform fields [27], [28]. Our ability, however, to view the same region from different angles both to characterize the scene type and to validate the theoretical model predictions has as yet been extremely limited.

MISR will constitute a major advance in our understanding of these problems by enabling direct validation of theoretical BRDF models. Multiangle imaging of globally distributed cloudy regions at high resolution will allow accurate cloud scene classifications and enable theoretical models to be applied to regional albedo and cloud property retrievals with far greater confidence than previously possible.

D. Terrestrial Ecosystems

About 30 percent of the Earth's surface is covered by land and much of this is vegetated. Thus, land surface processes are important components of the terrestrial climate system [29]. Sato *et al.* [30] have shown how the inclusion of a vegetation component in an atmospheric general circulation model greatly improves the realism of the calculated fluxes and the simulation of rainfall in the continental interiors. Sellers *et al.* [31] discussed how vegetation spectral, structural, and physiological properties in large part determine the fluxes of energy, mass, and momentum between the land surface and the atmosphere. Energy and mass transfer, in particular, are strong functions of biophysical processes such as photosynthesis and evapotranspiration. The maximum rate of CO_2 assimilation during photosynthesis and control over the throughput of transpired H_2O are governed by the photosynthetic capacity and minimum canopy resistance, respectively, which are strongly correlated with the canopy spectral hemispherical albedo [32]–[34]. This albedo cannot be estimated with an accuracy of better than about 45 percent from nadir spectral reflectance; even when physical models of the canopy are invoked the accuracy cannot be improved to better than about 25 percent [34]. Meaningful estimates will require the acquisition of multiangle data.

The time-evolution of terrestrial ecosystems is difficult to monitor at the surface and satellite platforms provide a unique opportunity to carry out extensive surveys with comprehensive spatial coverage and high time resolution. The detection of ecophysiological change necessitates accurate, repeatable measurements of the surface that can be used for landscape classification. Such monitoring is important if we are to 1) determine the level of direct anthropogenic impact on the land biota and 2) detect species compositional "drift" in response to environmental perturbations, whether natural or anthropogenic in origin. Although spectral data provide some information on the physiological state of vegetation, inference of the structural properties of the three-dimensional vegetation stand is also required, and it is almost impossible to determine any knowledge of canopy architecture and states (e.g., biomass, leaf area index) from a single view angle [35], [36].

MISR will provide estimates of radiative energy fluxes over vegetated terrain with accuracies unattainable with nadir-viewing sensors, thereby facilitating needed improvements in the boundary conditions of general circulation and climate models. Since spectral information alone is a poor discriminator of vegetation canopy architecture, MISR, in conjunction with high temporal resolution observations from other sensors, will enable studies of the spatial distribution of vegetation community composition and species and its time rate of change.

III. Investigation Methodology

A. Aerosol Retrievals over Land

The aerosol optical properties that must be retrieved for climatology studies and atmospheric corrections are opacity τ, single-scattering albedo $\bar{\omega}_0$, and a size distribution metric, e.g., the exponent of a Junge (power law) distribution, ν. Diner and Martonchik [37] described how multiangle data from an instrument such as MISR could be used to retrieve τ. Their method makes use of the Lambert–Beer dependence of atmospheric transmittance with opacity and view angle and the prediction of three-dimensional radiative transfer (3DRT) theory that spatial variations in the TOA diffuse radiance are considerably smoother than those in the direct field due to scattering-induced blurring effects [17], [19]. This permits spatial Fourier filtering of the diffuse radiance and using the remaining signal to retrieve τ. As an example of this concept, a computer simulated MISR data set of eight images, one at each MISR view angle (25.8°, 45.6°, 60.0°, and 72.5° at two azimuth angles) was generated for a single wavelength (550 nm). The complex surface spatial structure of natural terrain was obtained by using radiometrically calibrated Landsat Thematic Mapper imagery degraded to the MISR resolution (in this example, a 256 × 256 pixel image of the Pasadena, California area) to which a first-order atmospheric correction was applied. The resulting pixel values were then interpreted to be surface hemispherical albedos to which normalized BRDF's from an empirical field data set [38], [39] were assigned. In this manner a simulated, nonlambertian surface scene containing several different BRDF's was specified. The atmosphere above the surface scene was modeled as horizontally homogeneous with both molecular and aerosol opacity. The molecular Rayleigh scattering component had an opacity of 0.10 and a scale height of 8 km; the aerosol component had an opacity of 0.21, a single-scattering albedo of unity, a phase function asymmetry parameter of 0.51, and a scale height of 2 km. Of these

parameters, the technique is sensitive only to the total opacity. Fig. 1 is a histogram of the 256 opacities retrieved by Fourier transforming the eight images line-by-line. The mean value determined from the retrieval algorithm is the correct total opacity (0.31) and the spread in the histogram is due primarily to the nonlambertian reflectance of the surface.

A promising technique for retrieving $\bar{\omega}_0$ is described by Fraser and Kaufman [40], who have studied the effects of different aerosol properties on the "critical reflectance" r_c or value of surface reflectance at which the TOA radiance is insensitive to changes in aerosol opacity. Since r_c is a function of $\bar{\omega}_0$, correlation of imagery obtained on clear and hazy days yields a measurement of r_c from which $\bar{\omega}_0$ can be calculated. Kaufman [41] pointed out that the method is more sensitive when off-nadir imagery is acquired, particularly for the lower single-scattering albedos characteristic of urban areas. These studies also show how collection of multiangle imagery on dates characterized by different opacities also provides sensitivity to the aerosol size distribution exponent ν. We are also investigating additional methods for retrieving $\bar{\omega}_0$ and ν, based extensively on the multiangle and spectral character of the anticipated MISR data.

The unique multiangle design of MISR will enable the development and implementation of techniques to retrieve aerosol properties for climate impact studies, environmental monitoring, and atmospheric correction schemes over land surfaces.

B. Aerosol Retrievals over Oceans

The algorithms developed for atmospheric corrections of CZCS imagery provide the product of the aerosol scattering phase function $P(\Theta)$, evaluated at the particular scattering angle Θ appropriate to the viewing geometry, and the opacity τ [20]. Since $P(\Theta)$ depends only weakly on wavelength λ, the radiance backscattered out of the ocean can be estimated with sufficient accuracy at $\lambda >$ 500 nm to determine the relative spectral variation of τ. This, in turn, provides a good estimate of the gross features of the aerosol size distribution [42], although a scattering model (e.g., Mie theory) and an estimate of the refractive index n of the aerosol are needed to calculate the *absolute* values of $P(\Theta)$ and τ. For the simplest case, the marine aerosols (generated by breaking waves) are spherical droplets composed of liquid water (with some dissolved salt) and the estimate of τ is routine. However, there is no mechanism to guarantee the validity of the assumptions used to derive τ, since the aerosol may be continental-type with a large index ($n \approx 1.55$) or may consist of irregularly shaped particles for which Mie theory is inapplicable.

By measuring $\tau P(\Theta)$ at several scattering angles and wavelengths, MISR will furnish estimates of τ over the ocean with significantly more confidence. Comparison of the phase function shape over a wide range of angles with Mie theory predictions will provide a test of the realism of the simple (spherical water droplet) model. The need

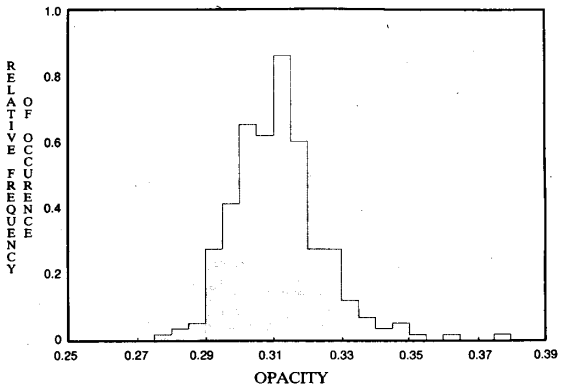

Fig. 1. Histogram of the 256 opacity values retrieved from each line of a simulated MISR image set. The correct value of opacity is 0.31.

for a slightly higher index to bring the model and observations into agreement would imply a greater concentration of dissolved salt [43]. However, if a high n is required, or if no "reasonable" index can be found, the aerosol must differ significantly from water and probably consists of nonspherical particles.

After experience has been gained working with MISR data, the phase function "signatures" of various aerosol types, e.g., continental, urban, African dust, etc., will be determined by examining imagery known to contain such species. Coupling these observations with simultaneous surface measurements of τ will yield $P(\Theta)$. Once the phase function "signature" is determined, analysis of aerosols over the ocean will include many of the known aerosol types and remove the restriction to solely marine aerosols. When this is accomplished, global mapping of τ for the oceans can be made on a near-daily basis by using the narrow-swath MISR to "calibrate" the aerosol model used for the retrieval of τ over the wide swath observed by the Moderate Resolution Imaging Spectrometer (MODIS). This synergism between MISR and MODIS is at the heart of the Eos concept.

MISR data will provide a means of validating satellite determinations of marine aerosol opacities and will enable development of techniques for retrieving continental aerosol opacities over oceans.

C. Atmospheric Correction Scheme for Land Surface Scenes

The goal of any atmospheric correction scheme is the retrieval of surface reflectance from TOA radiances. For land scenes, this is in general not possible without invoking auxiliary information, namely, the optical properties (τ, $\bar{\omega}_0$, and ν) of the intervening aerosols. In addition, an inversion algorithm to process the imagery must be developed. At the high spatial resolution of an instrument such as the High Resolution Imaging Spectrometer (HIRIS), adjacency effects as well as the more commonly encountered diffuse radiance effects must be taken into consideration, particularly for water quality and biologi-

cal productivity studies in which the targets are of low intrinsic reflectance. As an example of these effects, we modeled the TOA radiance over a 2-km wide clear lake surrounded by brighter surface vegetation. Figs. 2 and 3 show the optical properties of the water, vegetation, and atmospheric scatterers assumed in the model. Using 3DRT theory [44], [45] we calculated the TOA spectrum of the water (see Fig. 4). This spectrum shows a steep rise in reflectance toward the blue and an apparent but erroneous vegetation content due to the adjacency effect. We conclude that atmospheric corrections of images acquired at high spatial resolution will require an inversion algorithm that incorporates 3DRT theory. Thus, this theory will be an integral component of aerosol and surface property retrieval schemes developed for MISR. Accurate retrievals will also depend on angular reflectance measurements of the scene in order to characterize the departure of the surface from lambertian behavior. Once the atmospheric optical properties are known, either an iteration-relaxation scheme or a direct inversion scheme can be used to obtain the parameters in the scene BRDF [46]. Both the relaxation and inversion methods make use of Fourier processing to simplify the convolution operations intrinsic to the 3DRT theory. Hemispherical albedo can then be calculated by numerical or analytical integration of the surface BRDF.

The MISR investigation will provide information necessary to implement atmospheric corrections of high-resolution sensor data in three regards: by developing methods to retrieve aerosol optical properties at the time the images are collected, by obtaining direct observations needed to model the angular reflectance signature of the surface, and by developing algorithms based on 3DRT theory.

D. Cloud Property Parameterizations

Reflected solar fluxes cannot be directly measured on a regional scale from satellite altitudes. Fluxes measured by wide-angle sensors correspond to areas $> 10^6$ km^2 in extent, within which the scene type is assuredly inhomogeneous. To investigate the role of clouds on climate, relatively homogeneous local scenes must be observed, necessitating narrow field-of-view (FOV) sensors such as MISR. Radiances from the same scene, measured more or less coincidentally at several different angles, can be directly integrated to yield the flux. To our knowledge, MISR will be unique in satisfying this requirement from space. However, earlier satellites pioneered the beginnings of this technique [47], [48]. In practice, numerical integration of MISR multiangle reflectances to obtain cloud hemispherical albedo will benefit from theoretical 3DRT models to predict the reflectance at angles not observed by the sensor. Current versions of such models [27] indicate that differences between the reflection functions of different cloud scenes are greatest in the nadir and at the limb, and are minimum for a view angle of $\sim 60°$. Fig. 5, from Davies [27], illustrates this dependence for a variety of model clouds. The curves were calculated

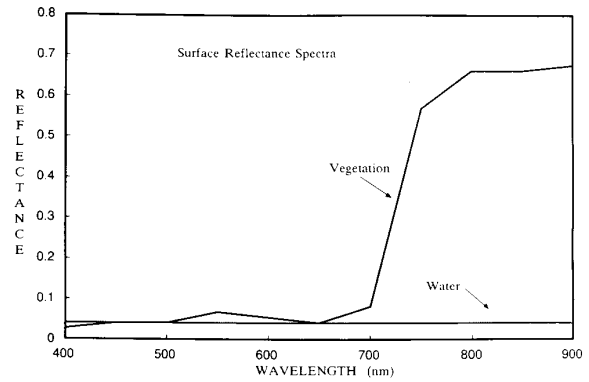

Fig. 2. Spectra of water and vegetation assumed in 3DRT adjacency effect simulation.

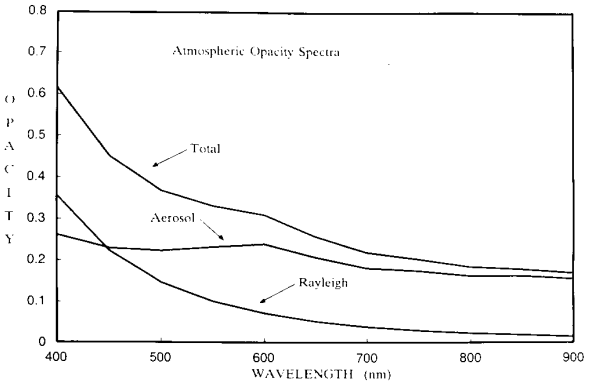

Fig. 3. Aerosol and Rayleigh scattering opacity spectra used in 3DRT adjacency effect simulation.

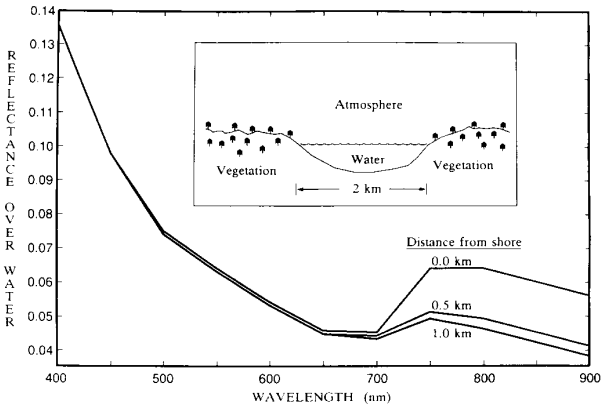

Fig. 4. Top-of-atmosphere spectra of clear water surrounded by vegetation, as a function of distance from shore. A signature of the vegetation is apparent due to the adjacency effect.

using a Monte Carlo radiative transfer algorithm and demonstrate the importance of obtaining measurements at angles both greater than and smaller than the critical 60° view angle in order to test the model predictions. Furthermore, methods of cloud classification (e.g., as stratiform, cumuliform, water, ice, etc.), based on spatial coherency between adjacent pixels [49] or parameterization

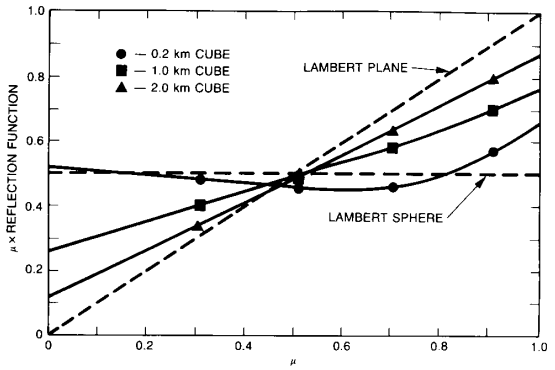

Fig. 5. Theoretical reflectance functions of cuboidal clouds of different sizes (adapted from [27]). Symbols are indicated at the values of μ, the cosine of the viewing angle, for which MISR will acquire images.

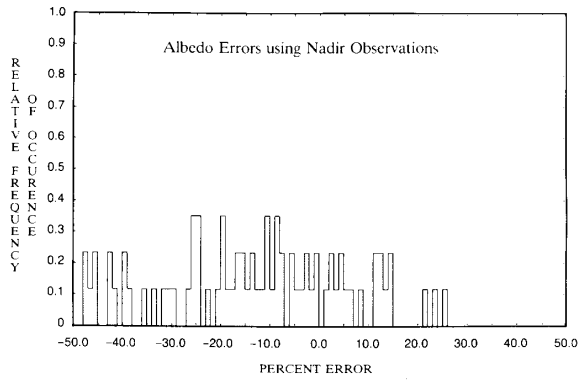

Fig. 6. Histogram of percent difference between nadir reflectance and hemispherical albedo, calculated using a field data set acquired by Kimes and coworkers [38], [39].

as mixtures of planar and spherical lambert reflectors [27], can also be tested, or new schemes developed.

As shown in theoretical simulations by Ridgway and Davies [50], the geometrical influence of clouds on broad-band reflected solar radiation is greatest for visible radiation, consistent with the spectral capabilities of MISR. This fact is due to the strong weighting of spectral cloud reflectivity to regions of minimal absorption by water (liquid or vapor). Since the absolute contribution of the rest of the solar spectrum to the broad-band reflected flux is far less dependent on geometrical variations in the cloud field, this contribution can be determined from the single-angle views of instruments with broad spectral coverage, such as HIRIS and MODIS. These instruments can thus be used synergistically with MISR to yield broad-band cloud albedos. For cloud systems of large areal extent, the relation between spectral and broad-band albedo can also be tested using data from MISR, MODIS, and the Eos Earth Radiation Budget Instrument (ERBI).

MISR will obtain measurements over a range of view angles necessary to obtain accurate estimates of cloud hemispherical albedo and test theoretical predictions of the angular variation of cloud reflectance. Methods of classifying and parameterizing cloud-filled scenes, including spatial coherency techniques and decomposition into contributions from lambert planes and spheres, will be explored.

E. Ecosystem Studies

Using simple models of canopy radiative transfer and leaf biophysics, several investigators [32]–[34], [51] showed that the upwelling irradiances observed above vegetated sites could yield relatively accurate information about rates of evapotranspiration, photosynthesis, respiration, and radiation absorption. Current climatological and biogeophysical research is focused on rate rather than state variables for the land surface, primarily because the atmospheric component of biogeophysical models is influenced by the fluxes of energy and mass across the land-atmosphere interface. Kimes *et al.* [34] showed that uncertainties in estimates of photosynthesis, transpiration, and absorbed radiation rates are comparable to errors in the estimation of the spectral hemispherical albedo of vegetated surfaces. To assess MISR's ability to furnish accurate estimates of this quantity, we obtained a field data set acquired by Kimes and coworkers [38], [39] on 38 different surface covers, including soils, crops, and forests. Directional reflectance measurements were obtained at six view angles and five azimuths and integrated to yield hemispherical albedo as described in Kimes and Sellers [35]. Fig. 6 is a histogram of the percent difference between nadir reflectance and hemispherical albedo; clearly, nadir reflectance is a poor estimator of albedo due to the nonlambertian character of most natural scenes. After interpolating the directional reflectance data to the MISR angles and fitting with spherical harmonics, the azimuthally independent component was integrated to calculate hemispherical albedo. This model-independent method yields a substantial improvement in accuracy over the nadir data, as shown in Fig. 7. Results for azimuthal directions parallel, perpendicular, or halfway between the principal scattering plane are summarized in this single histogram. Thus, acquisition of even a few multiangle views results in an impressive ability to estimate the hemispherical albedo of real surfaces. Concurrent use of canopy models should increase the accuracy even further.

Although an integrated quantity such as hemispherical albedo provides much more accurate information about biophysical rates than about vegetation states (e.g., green leaf area index, leaf angle distribution function, etc.), several investigators [52]–[54] have argued on the basis of field measurements and three-dimensional vegetation canopy models that the directional reflectance *distribution* is diagnostic of such canopy structure variables. Gerstl and Simmer [36] have suggested that certain diagnostic features of canopy BRDF's are invariant to atmospheric effects, and thus can be used to infer canopy state. It is clear that existing single-view-angle optical systems can only provide a limited accuracy in the calculation of canopy geometric attributes. MISR will fill this void by pro-

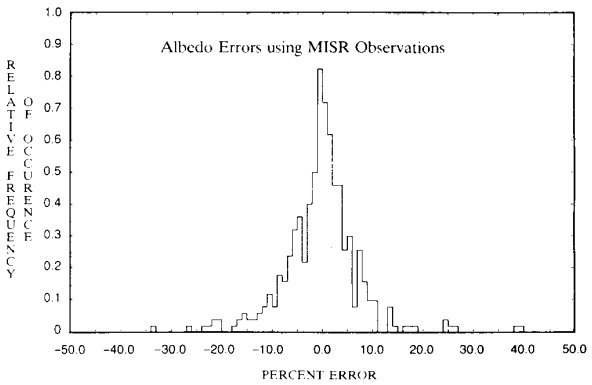

Fig. 7. Histogram of percent difference between hemispherical albedo estimated from data at the MISR view angles and the true values, calculated using the same data set as in Fig. 6.

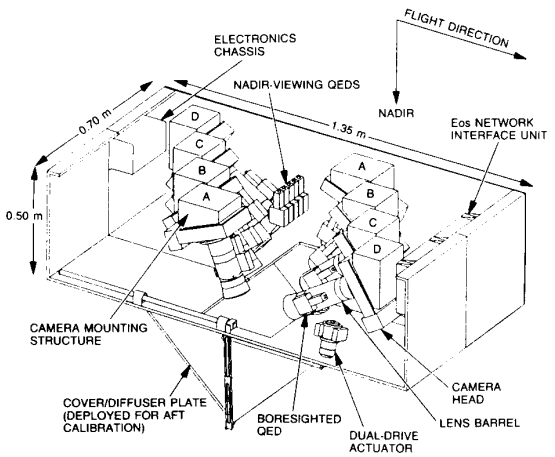

Fig. 8. Diagram of the MISR instrument conceptual design.

viding a global data set on the angular reflectance "signatures" of various classes of surface cover.

MISR observations will provide the ability to obtain accurate estimates of the hemispherical albedo of vegetated surfaces, which in turn will yield meaningful estimates of important biophysical rates. MISR directional reflectance images will enable the application of landscape classification and structural parameter retrieval techniques to a wide range of biomes.

IV. Measurement Strategy and Instrument Description

A. Angular Coverage

A diagram of the MISR instrument is shown in Fig. 8. It consists of eight separate pushbroom cameras that provide images at four different elevation look angles both forward and aftward of nadir in the direction of spacecraft travel. The fore and aft views furnish data at two azimuth angles relative to the solar illumination direction. In order to obtain view angles, θ, relative to the local normal at the Earth's surface of 25.8°, 45.6°, 60.0°, and 72.5°, the corresponding camera look angles from the Eos altitude of 824 km are 22.7°, 39.3°, 50.1°, and 57.6°. The cameras aimed at these angles are denoted by (*A*), (*B*), (*C*), and (*D*), respectively. Each of the cameras uses the same focal plane and camera body design coupled to one of four different types of telescope assembly. The cosines of the selected angles are 0.9, 0.7, 0.5, and 0.3; therefore, the angular coverage provides for uniform sampling in $\mu = \cos\theta$, an important parameter in radiation transfer studies. This strategy satisfies several objectives: 1) slant path observations through cloudless atmospheres are acquired out to airmass > 3, 2) cloud BRDF measurements at angles above and below the theoretical crossover point at $\theta \approx 60°$ are obtained, and 3) BRDF coverage of land, cloud, and water scenes necessary for structural modeling and for hemispherical albedo estimation is obtained.

B. Spatial Coverage and Resolution

Table I gives the first order properties of the MISR cameras (effective focal length, FOV, and clear aperture)

TABLE I
First-Order Properties of MISR Cameras

Camera	Effective focal length (mm)	Field-of-view	Clear aperture (mm)
A	63.2	27.4°	8.5
B	78.3	22.3°	10.5
C	100.0	17.5°	13.4
D	135.2	13.0°	18.3

and Fig. 9 shows the optical layouts. The cameras are designed independently to image a 443-km ground swath onto a 2048 element detector array. In each camera a 216-m ground pixel element maps to a 15-μm detector pixel element. Therefore, the FOV's and effective focal lengths vary with view angle while the f-numbers are held constant (at $f/8$) to preserve the etendue (area-solid angle product) between cameras. The optical layouts are scaled versions of the Double Gauss design with each camera optimized to achieve essentially diffraction limited performance. Color correction is accomplished by using FK54, a low index, ultra-low dispersion crystal, in the anastigmatic doublets.

It takes about 9 min of flight time for MISR to observe any given region at all eight view angles. The allocation of a separate camera to each view direction results in continuous multiangle imagery; consequently, MISR will obtain such imagery of the entire daylit Earth within the 16-day orbit repeat time of Eos. Including the ± 10 km uncertainty in Eos ground track repeatability and potential camera alignment errors, this requires a swath width of about 210 km. However, due to Earth rotation, a point viewed by the most forward-looking camera will have rotated eastward before being viewed by the lower-angle and aftward-looking cameras. The amount of eastward rotation is a function of latitude and is greatest at the equator. This is dealt with by acquiring imagery with a total swath width of 443 km. Making use of timing information to establish the spacecraft latitude, the appropriate 210-km subswaths are extracted from the data record by onboard editing under control of the instrument's micropro-

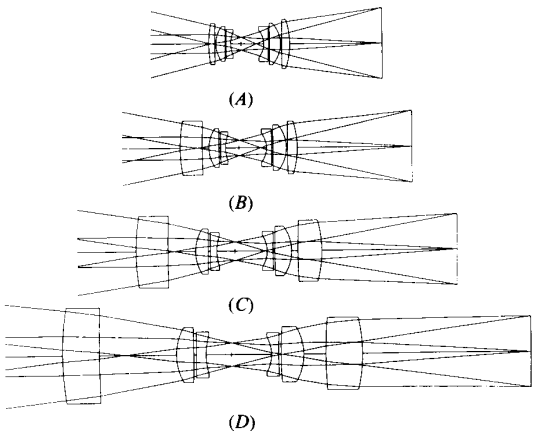

Fig. 9. Conceptual optical designs of the MISR cameras. (*A*), (*B*), (*C*), and (*D*) denote the cameras corresponding to view angles of 25.8°, 45.6°, 60.0°, and 72.5°, respectively.

cessor. This editing will be inhibited at selected times, e.g., during instrument calibrations.

C. Data Modes and Rates

For convenience, the global data set is divided into "frames," or sets of 32 images (eight view directions × four spectral bands). A frame measures 334 km along-track, thereby placing 60 frames between the orbit poles. MISR will observe in two resolution modes, defined by whether on-board pixel averaging is enabled. Global Mode data are generated by averaging data from eight adjacent pixels and eight successive lines, yielding images with a crosstrack pixel footprint and spacing of 1.73 km. This is the nominal imaging mode of MISR. To accomplish more detailed investigations, selected frames will be imaged with 216-m pixel spacing and crosstrack resolution (Local Mode) by inhibiting the on-board averaging for each of the eight cameras and placing a single camera at a time in that mode according to a predefined time sequence. A standard network of Local Mode scenes will be established, including sites for aerosol climatology studies, major cloud climatic regimes, major biomes, sites for field calibration and validation exercises, and sites selected for collaborative experiments with other Eos investigations. The MISR optical design enables matching of crosstrack footprint dimensions at all angles in both resolution modes. Depending on view angle, the downtrack footprint dimensions vary from 240–720 m (in Local Mode) and 1.92–5.76 km (in Global Mode) as a result of foreshortening; however, the line repeat time (33 ms) is the same for all cameras, resulting in identical sample spacings in both the crosstrack and downtrack directions (216 m in Local Mode and 1.73 km in Global Mode, assuming a spacecraft ground track velocity of 6.59 km/s). This sampling strategy enhances the scientific value of the data and permits correction for the variable downtrack resolution in the ground image processing software. Instrument data rates are 222 kbps in Global Mode and 2 Mbps in Local Mode. Occasionally, these rates will increase when swath editing is inhibited. The quantity of data anticipated per orbit is $\sim 10^9$ bits. The total data volume corresponds to an orbital average data rate of 164 kbps.

D. Spectral Coverage and Resolution

MISR imagery will be acquired in four spectral bands: 440, 550, 670, and 860 nm. The bandwidths (35, 20, 25, and 60 nm, respectively) are sufficiently narrow that spectral variations in aerosol optical properties over the band interval do not bias determinations of the band-averaged values and significant contamination by water vapor absorption is avoided. The bands in the red and near-infrared provide vegetated surface identification owing to their positioning on either side of the "red edge" marking the transition between chlorophyll absorption and cellulose reflectance. These two bands are also useful for marine aerosol studies since water is nearly black at these wavelengths. The band at 550 nm is near the peak of the solar spectrum. Finally, for determination of aerosol size distribution, the channel at 440 nm provides nearly a two-fold change in particle size-to-wavelength ratio relative to the channel at 860 nm.

The basic detector envisioned for the MISR cameras (Fig. 10) is a frame transfer charge coupled device (CCD) consisting of an image register containing four parallel sensor lines, a five-line storage register, and an output register [55]. The fifth line is used to obtain a transfer smear and dark current correction signal. This signal is transmitted along with the active data and used in the ground data processing. This detector was developed by RCA for the NASA Multispectral Linear Array (MLA) Program. The device has high quantum efficiency (ranging between 88 and 35 percent over the MISR spectral range). Each camera head will contain two CCD chips mosaicked into a 4 × 2048 active pixel array. Color filters are laminated to the CCD structure so that each of the four rows of pixels is filtered to one of the MISR wavelengths. This arrangement results in a small downtrack separation between the pushbroom images at the four wavelengths so that any point on the ground is imaged in succession in each of the spectral bands as the spacecraft moves down track. Spectral registration is handled after-the-fact in the ground data processing. The pixels are contiguous in the horizontal (2048 element) direction and the full well of each pixel is 10^6 electrons. Quantization noise at the 12-bit encoding is ~ 71 electrons rms. The detectors have a read noise floor of ~ 65 electrons rms and an average dark current of 825 electrons per integration.

E. Radiometric Performance

We anticipated that many observed scenes will be quite dark (e.g., aerosols over water) and others will contain high reflectance contrasts (e.g., clouds over ocean, inland lakes surrounded by bright terrain). It is therefore imperative that the instrument provide high sensitivity for a wide range of scene reflectance (0.1 to 100 percent) without

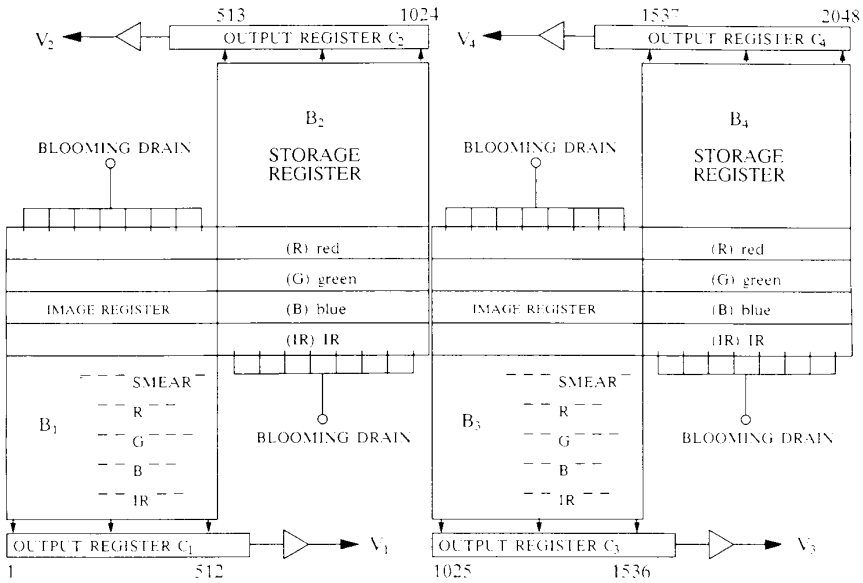

Fig. 10. Layout of the CCD planned for the MISR cameras (adapted from [55]).

TABLE II
PREDICTED SIGNAL-TO-NOISE RATIOS (SNR)

Equivalent reflectance	Average SNR (Local Mode)	Average SNR (Global Mode)
1.0	867	6850
0.1	260	1880
0.01	58	320
0.001	7	34

changes in gain. Using the MISR system parameters given above, the predicted instrument radiometric performance is given in Table II. Filter passbands were adjusted to give nearly wavelength invariant radiometric performance. The system performance is shown as a function of equivalent lambertian scene reflectance for both the Local and Global modes of operation. Global Mode pixels are 8 × 8 averages of Local Mode pixels; however, since the effect of pixel averaging on digitization noise is a function of other noise sources, Global Mode performance does not fully realize the potential eight-fold increase over Local Mode performance. Nevertheless, excellent performance is obtained over the range of MISR operation.

F. Calibration

The calibration requirements dictated by the MISR science objectives are deemed to be 3 percent absolute radiometric calibration, 0.5 percent relative within band radiometric calibration, 1 percent relative calibration between cameras and spectral bands, and ±5 nm spectral uncertainty. The absolute radiometry requirement is driven by the needs of the cloud and surface climatology communities, while the relative camera-to-camera and band-to-band radiometric precision requirements are driven by the desire to minimize instrumental errors in the determination of atmospheric opacity and the angular reflectance "signatures" of surfaces, clouds, and aerosol phase functions. To meet these goals, both source-based and detector-based preflight and inflight calibration techniques will be used. For example, the interior face of the instrument cover is bead-blasted aluminum prepared for use as a calibration surface. Such panels have been used on the Voyager spacecraft. The MISR panel is moved back and forth by a drive mechanism, first allowing calibration of the forward-viewing bank of cameras (over the North pole), then reoriented by 90° for calibration of the aftward-viewing cameras (over the South pole). For Earth viewing, the panel is moved out of the camera FOV's and stowed in a protected location. The diffuse calibration target and selected uniform targets on the Earth's surface will be monitored by 13 self-calibrating photodiode devices, or Quantum Efficient Detectors (QED's), such as the United Detector Technology QED-200. One QED will be boresighted with each camera, and five will be mounted on top of the instrument to obtain a nadir view of the target as shown in Fig. 8. Four of the five nadir viewing QED-200's will be color filtered with the same bandpasses as the CCD arrays. All of the remaining QED's will be operated in a broad-band mode. Each QED-200 consists of three silicon inversion-layer photodiodes arranged so that light reflected from one diode is absorbed by another diode. The output of each diode is summed in parallel resulting in an absolute accuracy of 0.1 percent.

Prior to flight, tests will be performed in order to measure the radiometric, spectral, spatial response, polarization, and noise characteristics of the instrument. In addition, any angular, spectral, and spatial nonuniformities of the panel will be measured and radiance values obtained using the nine broad-band QED's will be intercompared to verify precision. A comparison with source-based integrating sphere output values will be made to verify absolute calibration. For inflight operations, the incorporation of the diffuse calibration plate and QED detectors will enable the following redundant calibration modes:

1) *The radiance incident at the entrance pupil of each of the eight cameras is predicted during panel deployment using published solar irradiance data, computed illumination geometries, and preflight measured panel BRDF properties.*
2) *The QED detectors are used to directly measure solar reflected radiance from the diffuse panel. Degradations in panel reflectance are thus accounted for, assuming stable detector performance.*
3) *Radiances are computed for an overpass using field determined reflectances and measured atmospheric characteristics along with a radiative transfer code to predict radiances for a typical Local Mode scene. This calibration is independent of the diffuse panel and QED detector components, and should verify their performance.*
4) *Field data are used to compute broad-band and within-band radiances for validation of QED performance.*

G. Validation

Field tests will be conducted to verify performance of the in-orbit calibration system and validate retrieved surface and atmospheric parameters. When possible, tests will be done in conjunction with other instrument calibration exercises. Measurements will include narrow-band solar photometry to characterize aerosol, ozone, and molecular scattering during the time of the overflight, and surface BRDF characterization. The radiometer used to characterize the surface will be equipped with MISR filters and will reference output counts to a Halon calibration panel.

Validation of MISR calibration and data analysis algorithms to retrieve aerosol opacities and size distributions as well as cloud and surface BRDF's and albedos includes activities that can be done routinely at Science Team members' home institutions. For example, monitoring of aerosol optical properties can be done at JPL using existing radiometers and vertical profiles can be determined with ground-based lidar. Ground-based radiometric studies of clouds will be performed at McGill University. A monitoring station containing cloud doppler radar, surface radiometers, microwave profiler, radiosonde receiver, acoustic sounders, wind profilers, ceilometer, and sun-tracking photometer is currently being established at Pennsylvania State University. Relationships between angular signatures and surface structural properties and classifications will also be investigated in the laboratory by experimenting with artificial surfaces having predetermined and well-known BRDF characteristics. A structure to simulate vegetated canopies is currently being developed at Los Alamos National Laboratory.

H. Spacecraft Accommodation Requirements

With the exception of the detectors, which operate at 27°C, the MISR instrument operates at 20°C. The thermal design concept utilizes passive thermal control, with a radiator having a surface area of 0.8 m^2 located on the bottom of the instrument. The input power required to operate MISR is estimated to be 77 W. The driver motor of the cover/calibration panel requires an additional 18 W; however, it is used infrequently. The total instrument mass is estimated to be 75 kg. Instrument dimensions are shown in Fig. 8.

V. Data Products

A. Data Processing

Processing of MISR data will occur at a Central Data Handling Facility (CDHF) established by the Eos Project. Software development for bulk data processing at the CDHF will be conducted at the Image Processing Laboratory (IPL) at JPL. In addition, a MISR Data Quality and Performance Analysis Laboratory (DQPAL) will be established as a subsystem of IPL, for the purposes of analyzing the data quality, processing characteristics, and the long-term performance of the instrument. A MISR Science Data Analysis Facility (SDAF) will be established and used to develop and validate data analysis algorithms to be used for producing high-level standard data products and to perform nonstandard special-purpose science analysis of the MISR data. The SDAF concept is envisioned to be a mini-supercomputer networked with image display workstations.

B. Data Product Level Definitions and Processing Steps

Definition of the MISR data product levels follows, to the extent possible, the general Eos scheme from Level 0 to 4, although there are several significant differences. Level 0 consists of raw data and associated ancillary data are combined into a single, basic data product. At Level 1A, the data are reformatted and annotated with ancillary data that will be used in later processing steps. Calibration data are used to radiometrically calibrate the input data. Additionally, the data are geographically referenced using the ephemeris file that is converted to geographic coordinates linked to a pixel coordinate system. At Level 1B1, the data are geometrically rectified to remove the systematic image distortions that are due to lens distortions and Earth curvature. At Level 1B2, the data from the four spectral bands are geometrically registered using cross-correlation. Geometrically registered multiangle imagery of the eight MISR cameras comprises Level 1B3 data. A digital terrain model of the Earth will be used to correct for angle-dependent spatial shifts resulting in par-

allax over scenes with significant topographic relief. At Level 2, data acquired in one 16-day cycle are reprojected to a global map projection. Level 3 data consist of geometrically registered Local Mode land data acquired on subsequent orbital paths of the same area on the Earth. Level 4 products will result from application of model-dependent processing to MISR data.

C. Data Products

Archived products from the MISR experiment fall into several general categories. Category I consists of the annotated and reformatted data records processed through Level 1A. No irreversible processing will have been performed on these data. Category II products are TOA radiance images. The processing levels required to generate Category II products are 1B3, for registered multispectral, multiangle images; and Level 3 for temporally registered Local Mode land surface images. Data products will consist of scenes in four spectral bands and eight viewing geometries (i.e., 32 images), with an associated parameter file describing viewing conditions such as time of observation, image geography, and Sun geometry. Category III products are geophysical variables that can be derived on a pixel-by-pixel basis from the radiances within that pixel alone, more or less independently of neighboring pixel radiances or auxiliary information. Products falling into this category are processed through Level 2 and include planetary albedo maps in each of the four MISR spectral bands. Category IV products require processing through Level 4 and require contextual processing of the MISR data in which pixel-to-pixel variations must be analyzed in order to derive the final product. Procedures involving Fourier processing, such as aerosol retrievals and atmospheric corrections, fall into this category. Category IV products include global aerosol opacity and size distribution maps and global land surface climatology maps, such as maps of surface albedoy. The latter will require atmospheric corrections in their derivation. Category V, or specialized products, are those products that are not amenable to bulk data processing operations. Currently envisioned specialized products for the MISR experiment include a library of angular signature maps for various scene classes, such as vegetated landscapes and cloud systems. The total archived data volume from MISR is estimated to be 4 GByte/day. Optical disk storage will be needed to handle this volume of information.

VI. Conclusions

Theoretical simulations, ground-based measurements, and remotely sensed observations of aerosol-laden atmospheres, cloud fields, and vegetated landscapes demonstrate the necessity of multiangle data for climatological and biogeophysical studies. Multiangle imaging with MISR from Eos will enable thorough investigations of:

1) Climatic and environmental impacts of natural and anthropogenic aerosols

2) Climatic effects of heterogeneities in cloud fields

3) Land surface phenomena requiring accurate atmospheric corrections

4) Interactions between vegetation and atmospheric/climatological processes

5) Ecological changes resulting from natural and anthropogenic activities.

MISR will complement several Eos facility instrument investigations. The multiangle data can be combined with the high spatial and spectral resolution of HIRIS to enable detailed cloud studies as well as accurate atmospheric corrections needed for certain surface science disciplines; with the synoptic coverage of MODIS to extend the MISR capabilities to near-daily temporal resolution; and with the bolometric, coarsely sampled data from ERBI to obtain high-resolution broad-band planetary albedo images of the Earth. Because of these synergisms, we have proposed MISR for the Eos-1 platform.

Acknowledgment

The authors thank O. Chen, V. Ford, L. E. Hovland, and A. H. Vaughan for their contributions to this effort. We also thank P. A. Levine of the David Sarnoff Research Center for helpful discussions regarding the CCD detector and D. S. Kimes of Goddard Space Flight Center for providing us with his BRDF field data set on computer tape.

References

[1] S. J. Williamson, *Fundamentals of Air Pollution*. Reading, MA: Addison-Wesley, 1972.

[2] O. B. Toon and J. B. Pollack, "A global average model of atmospheric aerosols for radiative transfer calculations," *J. Appl. Meteorol.*, vol. 15, p. 225, 1976.

[3] D. Hoffman, "Aerosols from past and present volcanic emissions," in *Aerosols and Climate, Proc. IAMAP Symp. Aerosols and Climate*, XIX General Assembly of the IUGG. Hampton, VA: A. Deepak, 1988.

[4] J. B. Pollack, O. B. Toon, C. Sagan, A. Summers, B. Baldwin, and W. Van Camp, "Volcanic explosions and climatic change: a theoretical assessment," *J. Geophys. Res.*, vol. 81, p. 1071, 1976.

[5] G. L. Potter and R. D. Cess, "Background tropospheric aerosols: Incorporation with a statistical-dynamical climate model," *J. Geophys. Res.*, vol. 89, p. 9521, 1984.

[6] R. S. Kandel, *Earth and Cosmos*. Oxford, Pergamon, 1980.

[7] J. T. Peterson, E. C. Flowers, G. J. Beni, C. L. Reynolds, and J. H. Rudisill, "Atmospheric turbidity over central North Carolina," *J. Appl. Meteorol.*, vol. 20, p. 229, 1981.

[8] G. E. Shaw, "Atmospheric turbidity in the polar regions," *J. Appl. Meteorol.*, vol. 21, p. 1080, 1982.

[9] A. P. Waggoner, R. E. Weiss, N. C. Ahlquist, D. S. Covert, S. Will, and R. J. Charlson, "Optical characteristics of atmospheric aerosols," *Atmos. Environ.*, vol. 15, p. 1981, 1981.

[10] T. P. Ackerman and O. B. Toon, "Absorption of visible radiation in atmosphere containing mixtures of absorbing and nonabsorbing particles," *Appl. Opt.*, vol. 20, p. 3661, 1981.

[11] J. T. Suttles and G. Ohring, "Workshop on surface radiation budget for climate applications," World Climate Research Program, WCP-115, WMO/TD-No. 109, Columbia, MD, 1986.

[12] F. P. J. Valero and T. P. Ackerman, "Arctic haze and the radiation budget," in *Arctic Air Pollution*, B. Stonehouse, Ed. Cambridge: Cambridge, 1986.

[13] T. P. Ackerman, "Aerosols in Climate Modeling," in *Aerosols and Climate, Proc. IAMAP Symp. Aerosols and Climate, XIX General Assembly of the IUGG*. Hampton, VA: A. Deepak, 1988.

[14] R. S. Fraser, "Satellite measurement of mass of Sahara dust in the atmosphere," *Appl. Opt.*, vol. 15, p. 2471, 1976.

[15] R. S. Fraser, O. P. Bahethi, and A. H. Al-Abbas, "The effect of the

atmosphere on the classification of satellite observations to identify surface features," *Remote Sensing Environ.*, vol. 6, p. 229, 1977.
[16] R. P. Jackson, P. N. Slater, and P. J. Pinter, "Discrimination of growth and water stress in wheat by various vegetation indices through clear and turbid atmospheres," *Remote Sensing Environ.*, vol. 13, p. 187, 1983.
[17] W. A. Pearce, "A study of the effects of the atmosphere on Thematic Mapper observations," Rep. 004-77, EG&G Washington Analytical Service Center, Riverdale, MD, 1977.
[18] Y. J. Kaufman, "Atmospheric effect on spatial resolution of surface imagery," *Appl. Opt.*, vol. 23, p. 3400, 1984.
[19] D. J. Diner and J. V. Martonchik, "Influence of aerosol scattering on atmospheric blurring of surface features," *IEEE Trans. Geosci. Remote Sensing*, vol. GE-23, p. 618, 1985.
[20] H. R. Gordon, D. K. Clark, J. W. Brown, O. B. Brown, R. H. Evans, and W. W. Broenkow, "Phytoplankton pigment concentrations in the Middle Atlantic Bight: comparison of ship determinations of CZCS estimates," *Appl. Opt.*, vol. 22, p. 20, 1983.
[21] M. Griggs, "Measurements of atmospheric aerosol optical thickness over water using ERTS-1 data," *J. Air Pollut. Control Assoc.*, vol. 25, p. 622, 1975.
[22] Y. H. Mekler, Quenzel, G. Ohring, and I. Marcus, "Relative atmospheric aerosol content from Erts observations," *J. Geophys. Res.*, vol. 82, p. 967, 1977.
[23] Y. P. Kaufman and J. H. Joseph, "Determination of surface albedos and aerosol extinction characteristics from satellite imagery," *J. Geophys. Res.*, vol. 87, p. 1287, 1982.
[24] T. Lee and Y. J. Kaufman, "The effect of surface non-Lambertianity on remote sensing," *IEEE Trans. Geosci. Remote Sensing*, vol. GE-24, p. 699, 1986.
[25] R. M. Welch and B. A. Wielicki, "Stratocumulus cloud field reflected fluxes: The effect of cloud shape," *J. Atmos. Sci.*, vol. 41, p. 3085, 1984.
[26] Harshvardhan, R. Davies, D. A. Randall, and T. G. Corsetti, "A fast radiation parameterization for atmospheric circulation models," *J. Geophys. Res.*, vol. 92, p. 1009, 1987.
[27] R. Davies, "Reflected solar radiances from broken cloud scenes and the interpretation of scanner measurements," *J. Geophys. Res.*, vol. 89, p. 1259, 1984.
[28] J. A. Coakley and R. Davies, "The effect of cloud sides on reflected solar radiation as deduced from satellite observations," *J. Atmos. Sci.*, vol. 43, p. 1025, 1986.
[29] R. E. Dickinson, "Land surface processes and climate-surface albedos and energy balance," *Adv. Geophys.*, vol. 25, p. 305, 1983.
[30] N. Sato, P. J. Sellers, D. A. Randall, E. K. Schneider, J. Shukla, J. L. Kinter III, and Y.-T. Hou, "Effects of implementing the Simple Biosphere model (SiB) in a general circulation model," submitted to *J. Atmos. Sci.*, 1988.
[31] P. J. Sellers, Y. Mintz, Y. C. Sud, and A. Dalcher, "A Simple Biosphere model (SiB) for use within general circulation models," *J. Atmos. Sci.*, vol. 43, p. 305, 1986.
[32] P. J. Sellers, "Canopy reflectance, photosynthesis and transpiration," *Int. J. Remote Sensing*, vol. 8, p. 1335, 1985.
[33] ——, "Canopy reflectance, photosynthesis and transpiration II: The role of biophysics in the linearity of their interdependence," *Remote Sensing Environ.*, vol. 21, p. 143, 1987.
[34] D. S. Kimes, P. J. Sellers, and D. J. Diner, "Extraction of spectral hemispherical reflectance (albedo) of surfaces from nadir and directional reflectance data," *Int. J. Remote Sensing*, vol. 8, p. 1727, 1987.
[35] D. S. Kimes and P. J. Sellers, "Inferring hemispherical reflectance of the Earth's surface for global energy budgets from remotely sensed nadir or directional radiance values," *Remote Sensing Environ.*, vol. 18, p. 205, 1985.
[36] S. A. W. Gerstl and C. Simmer, "Radiation physics and modeling for off-nadir satellite-sensing of non-lambertian surfaces," *Remote Sensing Environ.*, vol. 20, p. 1, 1986.
[37] D. J. Diner and J. V. Martonchik, "Atmospheric transmittance from spacecraft using multiple view angle imagery," *Appl. Opt.*, vol. 24, p. 3503, 1985.
[38] D. S. Kimes, "Dynamics of directional reflectance factor distributions for vegetation canopies," *Appl. Opt.*, vol. 22, p. 1364, 1983.
[39] D. S. Kimes, W. W. Newcomb, C. J. Tucker, I. S. Zonneveld, G. F. Epema, and J. de Leeuw, "Directional reflectance factor distributions for cover types of northern Africa in NOAA 7/8 AVHRR Bands 1 and 2," *Remote Sensing Environ.*, vol. 18, p. 1, 1985.
[40] S. R. Fraser and Y. J. Kaufman, "The relative importance of aerosol scattering and absorption in remote sensing," *IEEE Trans. Geosci Remote Sensing*, vol. GE-23, p. 625, 1985.
[41] Y. J. Kaufman, "Satellite sensing of aerosol absorption," *J. Geophys. Res.*, vol. 92, p. 4307, 1987.
[42] H. R. Gordon, "Some studies of atmospheric optical variability in relation to CZCS atmospheric correction," NOAA National Environmental Satellite and Data Information Service, Final Rep. Contract NA-79-SAC-00714, 1984.
[43] H. Quenzel and M. Kaestner, "Optical properties of the atmosphere: Calculated variability and application to satellite remote sensing of phytoplankton," *Appl. Opt.*, vol. 19, p. 1338, 1980.
[44] D. J. Diner and J. V. Martonchik, "Atmospheric transfer of radiation above an inhomogeneous non-lambertian reflective ground. I. Theory," *J. Quant. Spec. Rad. Transf.*, vol. 31, p. 97, 1984.
[45] ——, "Atmospheric transfer of radiation above and inhomogeneous non-lambertian reflective ground. II. Computational considerations and results," *J. Quant. Spec. Rad. Transf.*, vol. 32, p. 279, 1984.
[46] D. J. Diner, J. V. Martonchik, E. D. Danielson, and C. J. Bruegge, "Application of 3-D radiative transfer theory to atmospheric correction of land surface images," *Int. Geosci. Remote Sensing Symp.* (Edinburgh, Scotland), 1988.
[47] V. R. Taylor and L. L. Stowe, "Reflectance characteristics of uniform Earth and cloud surfaces derived from Nimbus-7 ERB," *J. Geophys. Res.*, vol. 89, p. 4987, 1984.
[48] G. L. Smith, R. N. Green, E. Raschke, L. M. Avis, J. T. Suttles, B. A. Wielicki, and R. Davies, "Inversion methods for satellite studies of the Earth's radiation budget: Development of algorithms for the ERBE mission," *Rev. Geophys.*, vol. 24, p. 407, 1986.
[49] J. A. Coakley and F. P. Bretherton, "Cloud cover from high-resolution scanner data: Detecting and allowing for partially filled fields of view," *J. Geophys. Res.*, vol. 87, p. 4917, 1982.
[50] W. L. Ridgway and R. Davies, "Interpretation of spectral reflection from cloud tops," in *Proc. 5th Conf. Atmos. Radiation* (Amer. Meteor. Soc.), p. 501, 1983.
[51] C. J. Tucker and P. J. Sellers, "Satellite remote sensing of primary production," *Int. J. Remote Sensing*, vol. 7, p. 1395, 1986.
[52] J. A. Kirchner, D. S. Kimes, and J. E. McMurtrey III, "Variation of directional reflectance factors with structural changes of a developing alfalfa canopy," *Appl. Opt.*, vol. 21, p. 3766, 1982.
[53] D. S. Kimes, "Modeling the directional reflectance from complete homogeneous vegetation canopies with various leaf orientation distributions," *J. Opt. Soc. Amer.*, vol. 1, p. 725, 1984.
[54] N. S. Goel and R. L. Thompson, "Inversion of vegetation canopy reflectance models for estimating agronomics variables. V. Estimation of leaf area index and average leaf angle using measured canopy reflectances," *Remote Sensing Environ.*, vol. 16, p. 69, 1984.
[55] H. Elabd, A. D. Cope, F. V. Shallcross, W. F. Kosonocky, P. A. Levine, and D. M. Hoffman, "4 × 1024 CCD array for remote sensing applications," *J. Imaging Tech.*, vol. 11, p. 198, 1985.

*

David J. Diner received the B.S. degree in physics with honors from the State University of New York at Stony Brook in 1973 and the M.S. and Ph.D. degrees in planetary science from the California Institute of Technology, Pasadena, in 1977 and 1978, respectively.

He joined JPL as a National Research Council Resident Research Associate (NRC-RRA) in 1978 and was responsible for the development of data processing software for the Pioneer Venus Orbiter Infrared Radiometer. He continued these studies as a contractor with the Ball Aerospace Systems Division and became a JPL employee in 1981. He is currently a Technical Group Supervisor in the Atmospheric and Cometary Sciences Section. He has been an investigator in the NASA Planetary Atmospheres Program studying the temperature, aerosol, and cloud structure of Venus and Jupiter, and the NASA Land Processes Remote Sensing Science Program studying atmospheric effects on surface remote sensing. He also provides science support to the HIRIS Project at JPL. He is a member of the NASA Land Aircraft Science Management Operations Working Group.

Carol J. Bruegge received the B.A. and M.S. degrees in applied physics from the University of California at San Diego in 1978 and the M.S. and Ph.D. degrees in optical sciences from the University of Arizona, Tucson, in 1985.

Since joining JPL in 1985, she has been a Member of the Technical Staff in the Atmospheric and Oceanographic Sciences Section. Her experience is principally in the area of terrestrial remote sensing, radiative transfer, and use of ground-truth measurements for absolute radiometric calibration of remote sensing instruments, including the Landsat Thematic Mapper. Since 1987 she has applied these techniques to the calibration of the Airborne Imaging Spectrometer (AIS) and the Airborne Visible/Infrared Imaging Spectrometer (AVIRIS). She is currently a Principal Investigator in the First International Satellite Land Surface Climatology Program Field Experiment (FIFE) program, performing field experimentation to characterize the optical properties of the atmosphere and surface.

*

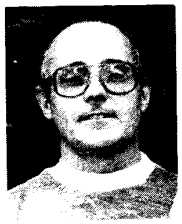

John V. Martonchik received the B.S. degree in physics from Case Institute of Technology in 1964 and the Ph.D. degree in astronomy from the University of Texas at Austin in 1974.

He joined JPL in 1972 and is currently a Member of the Technical Staff in the Atmospheric and Oceanographic Sciences Section. His experiences include telescopic and spacecraft observations of planetary atmospheres, laboratory and theoretical studies of the optical properties of gaseous, liquid and solid materials, and development and implementation of one- and three-dimensional radiative transfer and line-by-line spectroscopy algorithms for studies of planetary atmospheres and Earth tropospheric remote sensing. He is a coinvestigator in several NASA Land Processes programs including Remote Sensing Science and FIFE, and provides science support to the HIRIS project.

*

Thomas P. Ackerman received the B.A. degree in physics from Calvin College, Grand Rapids, MI, in 1970, and the M.Sc. degree in physics and the Ph.D. degree in atmospheric science from the University of Washington, Seattle, in 1971 and 1976, respectively.

For three years he worked at the Australian Numerical Meteorology Research Center and in 1979 he became a National Research Council Resident Research Associate (NRC-RRA) at NASA Ames. He subsequently took a civil service position that he held until 1988. He is currently Associate Professor of Meteorology and Associate of the Earth System Science Center at Pennsylvania State University, University Park. His research has included theoretical studies of the climatic impact of aerosols associated with pollution, volcanic eruptions, and catastrophic events (asteroid impacts and nuclear wars). He recently participated in the ACE program to study stratospheric aerosols; STEP, to study the role of clouds in stratospheric-tropospheric exchange processes; FIRE, to study impact of cirrus and marine stratus clouds on radiation budget; and the DNA fire research program, to look at smoke plumes from natural and prescribed forest fires.

Dr. Ackerman is a member of the FIRE Science Experiment Team, the DNA Advisory Committee on Field Experiments, the ISCCP/FIRE panel of the NRC Board of Atmospheric Sciences and Climate, and the AMS Committee on Radiative Energy. In 1985, he was awarded the Leo Szilard Award for Science in the Public Interest by the American Physical Society.

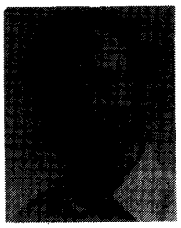

Roger Davies received the B.Sc. degree in physics with honors from Victoria University, Toronto, Ontario, in 1970 and the Ph.D. degree in meteorology from the University of Wisconsin at Madison in 1976.

He is currently Associate Professor of Meteorology at McGill University, where he lectures on atmospheric physics and the theory of climate, and directs a research laboratory on studies of clouds, radiation, and climate. He is a science team member of the Earth Radiation Budget Experiment (ERBE) and the First International Satellite Cloud Climatology Program Regional Experiment (FIRE).

Dr. Davies is a member of the Committee on Atmospheric Radiation of the American Meteorological Society and an Associate Editor of the *Journal of Geophysical Research* (Atmospheres).

*

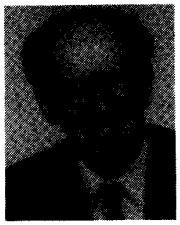

Siegfried A. W. Gerstl (M'86) received the B.S. and M.S. degrees in physics from the University of Stuttgart and the Ph.D. (Dr. rer. nat.) degree from the University of Karlsruhe in West Germany.

As a theoretical physicist and a senior engineer he developed new computational methods for the solution of the space-, energy-, and angular-dependent radiative transfer equation, applied originally to nuclear reactor shielding calculations, but more recently also applied to the transfer of solar and laser beam radiation through the atmosphere and other scattering and absorbing media. In 1980 he initiated a climatology research program at the Los Alamos National Laboratory with emphasis on radiative transfer through realistic atmospheres. His most recent contributions are to the physics of remote sensing of Earth surface features from satellite instruments, the theory of atmospheric correction algorithms, and modeling of atmospheric optics and imaging. As a member of the Imaging Spectrometer Science Advisory Group (ISSAG) he assisted NASA in defining the instrument requirements for HIRIS as documented in the HIRIS Instrument Panel Report. He has served as Principal Investigator for research projects sponsored by NASA, the EPA, the U.S. Army, the U.S. Air Force, and the DOE.

*

Howard R. Gordon received the B.S. degree in physics from Clarkson College of Technology, Potsdam, NY, in 1961. In 1963 and 1965 he received the M.S. and Ph.D. degrees, respectively, from Pennsylvania State University. Since 1976 he has been Professor of Physics at the University of Miami, Coral Gables, FL. His research interests include radiative transfer in the ocean-atmosphere system, development of atmospheric correction and chlorophyll concentration retrieval techniques for satellite ocean imaging, and validation of remote sensing products.

In 1977 Dr. Gordon was elected Fellow of the Optical Society of America, in 1982 he was awarded the NASA Public Service Medal, and in 1985 he participated in the NASA Public Service Group Achievement. He is currently a member of the NASA Color Science Working Group and the IAPSO Subcommission on Optics and Remote Sensing of the Ocean.

Piers J. Sellers received the B.Sc. degree in ecological science from Edinburgh University in 1976 and the Ph.D. degree in geography from Leeds University in 1981.

In 1982 he became a National Research Council Resident Research Associate (NRC-RRA) at the NASA Goddard Space Flight Center working on surface energy balance computer models. Since 1984 he has been a Faculty Research Scientist in the Department of Meteorology at the University of Maryland. He is undertaking research in atmosphere-biosphere interactions and remote sensing applications using computer simulation at the University of Maryland and GSFC. Since 1985 he has been a member of the International Satellite Land Surface Climatology Program (ISLSCP) Steering Committee under the sponsorship of WMO, UNEP, IAMAP, COSPAR, and NASA. In 1986 he became a member of the International Geosphere-Biosphere Program Planning Subcommittee for Terrestrial Ecosystems and in 1987 he became Staff Scientist for the First ISLSCP Field Experiment (FIFE).

*

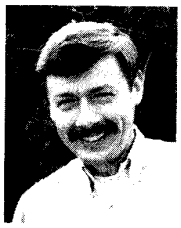

Jerry Clark received the B.S. and M.A. degrees in geography from San Diego State University, San Diego, CA, and California State University, Los Angeles, respectively.

He has been a member of the Image Processing Development and Applications Section at JPL for over 12 years, developing techniques for Earth resources applications of Landsat, Seasat, Shuttle Imaging Radar, and digital terrain data, using digital image processing and geographic information systems. He is currently coordinating preparations for the image processing of radar data from the upcoming Magellan spacecraft mission to Venus. His papers have primarily dealt with the creation of image data bases and the analysis of image data.

*

James A. Daniels received the B.E.E.E. degree from the University of Southern California, Los Angeles.

He worked for Northrop Aircraft Corporation on circuit design on the SNARK missile program in 1956 to 1964. From 1964 to 1972 he worked at JPL in design of circuits for space flight instruments. In 1972 he joined Bendix Corporation's Oceanic Division on their sonar programs, including the missile scoring system, active torpedo transmitter, and Dipped Sonar program for locating submarines. In 1984 he returned to JPL where he served as Task Manager on the Internal Discharge Monitor instrument for the CRRES satellite. In 1986 he joined the Imaging Section where he has worked on the Very High Speed and the Soft X-ray Telescope Cameras.

*

Eric D. Danielson received a Chemistry Research Fellowship at Principia College, Elsah, IL, (1983–1984) studying reflectance spectroscopy techniques, and in 1987 received the B.S. degree in general engineering from Harvey Mudd College, Claremont, CA.

He joined JPL in 1985 as an Academic Part-Time in the Atmospheric and Cometary Sciences Section, studying the sensitivity of surface reflectance to atmospheric effects. In 1987 he became a Contractor with the Merrie Computing Company, providing computer software and hardware support and maintenance to various NASA-supported research programs at JPL. He is proficient in many computing languages, including C, Fortran, Pascal, and Basic.

Valerie G. Duval received the B.S. degree in physics from New Mexico State University, Las Cruces, in 1981.

Upon joining the Infrared and Analytical Instrument Systems Section at JPL in 1981, she worked on the system design and analysis of an advanced orbital atmospheric temperature sounder. Subsequent to this activity, she became the Cognizant Engineer for the development of 2.5-μm-cutoff HgCdTe area array IR detectors for the High Resolution Imaging Spectrometer (HIRIS). Her work includes techniques for thermal imaging spectrometry, forest fire detection, and extrasolar planet detection. She is currently a member of the Technical Staff at JPL.

*

Kenneth P. Klaasen is the Supervisor of the Imaging Science Group at JPL. He received the B.S. degree in physics from the University of Michigan, Ann Arbor, in 1969.

He has been involved in many solar system exploration missions including Mariner 10, Viking Orbiter, and currently the Galileo mission to Jupiter. He has served as Experiment Representative for the imaging experiments on these missions and is currently a member of the Galileo Imaging Science Team. His primary responsibilities have included imaging system calibration, experiment planning, and mission operations. He has published papers on the rotation period of Mercury, Venus atmospheric dynamics, and the photometry of Mercury, Mars, and the martian moons Phobos and Deimos, as well as several on various spacecraft imaging instruments and experiments.

*

Gerald W. Lilienthal is an Engineer in the System Integration Section of JPL. He has seven years of experience in the research, design, and development of mechanisms products spanning the range from compressors to tape recorders to spacecraft devices. He holds several patents.

*

David I. Nakamoto received the B.S.E.E. degree in 1981 from the California Polytechnic University of Pomona.

He joined General Dynamics of Pomona in 1981, working on flight signal processing software and guidance system testing and integration. He joined JPL in 1984 where his work includes real time testing of spacecraft guidance systems, design of ground support equipment, and development of systems to handle in-flight real time data processing.

Robert J. Pagano received the B.S. degree in optics in 1985 and the M.S. degree in optics in 1986 from the University of Rochester, Rochester, NY.

He is currently a Member of the Technical Staff in the Optical Sciences Group, Optical Sciences and Application Section of the JPL Observational Systems Division. His experience includes optical design and testing. Since he joined JPL he has provided optical testing support to the Large Deployable Reflector (LDR) project and is currently the Optical Designer for the Atmospheric Infrared Sounder (AIRS) instrument for the Eos platform and the Probe Infrared Laser Spectrometer (PIRLS) for the Cassini mission.

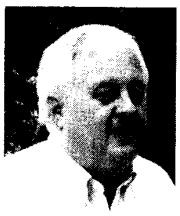

Terrence H. Reilly received the Ph.D. degree in solid-state physics from the Institute of Optics at the University of Rochester, Rochester, NY.

He joined JPL in 1969, and was a member of the imaging system development teams for several flight missions: Mariner Venus/Mercury, Viking Orbiter, and Voyager. He was appointed a Technical Group Supervisor in 1975, and was assigned responsibility for optics, camera heads, and mechanisms for the Space Telescope Wide Field/Planetary Camera. He joined the Government Systems Division at Eastman Kodak in 1985, where he was supervisor of a new electro-optics laboratory. He recently returned to JPL, and is presently a Technical Group Supervisor in the Imaging System Section. He has published eight technical papers and holds one patent for a medical imaging system.